JOURNAL OF Applied Polymer SCIENCE

Electrically Conductive Adhesive Based on Bismaleimide-Triazine Resin Filled with Microcoiled Carbon Fibers

Guanglei Wu, Kaichang Kou, Ning Li, Hailin Shi, Min Chao
School of Science, Northwestern Polytechnical University, Xi'an 710129, People's Republic of China
Correspondence to: K. Kou (E-mail: happywu1028@yahoo.com.cn)

ABSTRACT: Electrically conductive adhesive (ECA) was prepared with cyanate ester resin and bismaleimide resin formed bismaleimide-triazine resin as the matrix, a γ-glycidoxy propyl trimethoxy silane (KH-560) as the coupling agent, and the carbon microcoils (CMCs) as the conducting filler. CMCs were synthesized by the catalytic decomposition of acetylene using nickel sulfide particles as the catalyst, which prepared by solvothermal method. The morphology and microstructure of CMCs were examined by scanning electron microscopy, Fourier transform infrared spectroscopy, and X-ray diffraction. The electrical conductivity of the ECA increased to 3.16×10^{-2} S/cm. When the content of CMCs was 1.5 wt %, the shear strength between 25 and 200°C remained at a high value of 22.8 and 21.4 MPa, respectively. © 2012 Wiley Periodicals, Inc. J. Appl. Polym. Sci. 000: 000–000, 2012

KEYWORDS: adhesives; mechanical properties; X-ray; catalysts; blends

Received 19 April 2012; accepted 11 July 2012; published online
DOI: 10.1002/app.38348

INTRODUCTION

Tin/lead (Sn/Pb) solders have been used as electrical interconnects in most areas of electronic packaging. Lead, one of the components in solder, has long been recognized as a health threat to human beings.[1] In addition, worldwide regulations against the use of lead in electronics have been severe. Therefore, legislation and policies have been proposed in Europe to limit or ban the use of lead in solders, and similar action may be adopted by the United States.[2] Compared to Sn/Pb solders, electrically conductive adhesives (ECAs) provide a promising environmentally friendly solution for interconnections in electronic applications, flip chip assembly, smart card applications, chip scale package, and novel microsystems.[3,4] To expand the practical applications of ECAs, superior interconnect properties and reliability of the adhesives need to be realized through the assembly process.

Normally, high performance conductive adhesives were designed by combining the thermosetting resin and the effective electrically conductive fillers.[5–7] It was observed that carbon microcoils (CMCs) with the coil diameters of the micrometer order could be obtained by the catalytic pyrolysis of acetylene at 750–800°C.[8–10] Silver has the lowest electrical resistivity among single metals, and its oxide form is also conductive, unlike other metals. For these reasons, Ag has been primarily used as conductive fillers in conductive adhesive materials. Even so, the silver filler has one disadvantage of higher cost. The CMCs had a diversity of interesting three-dimensional helical/spiral structures, many excellent electrical and mechanical properties. There are many reports concerning the preparation of CMCs using various catalysts, such as metals supported on fine ceramic powders,[11,12] iron-coated indium tin oxide,[13] and coated on silicon and copper substrates.[14] Recently, studies of ECAs have been reported, most researches focused on epoxy resin[15] and silicone.[16] However, studies of ECAs which were consist of bismaleimide-triazine (BT) resin and CMCs were very limited. In this article, ECAs comprised BT with CMCs which prepared by blending method were obtained.

EXPERIMENTAL

Methods

Preparation of Sulfide Nickel Catalyst by Solvothermal Method. Sulfide nickel (NiS) catalysts were prepared by solvothermal method. First of all, the volume ratio of ethylene glycol and distilled water in the mixed solvent was 1 : 1. Then, 0.53 g nickel sulfate hexahydrate ($NiSO_4 \cdot 6H_2O$) and 0.19 g thiourea were added into the mixture with the stirring constantly. The mixture was suppressed into a reactor control system based on poly-tetrafluoroethylene (PTFE) inside linings. The reaction mixture was kept at 180°C for 12 h. Afterward, the sedimentation was filtered and washed with distilled water and ethanol. Then, it was dried at 50°C for 5 h. After cooling to room temperature, the NiS catalyst was obtained.

Applied Polymer SCIENCE

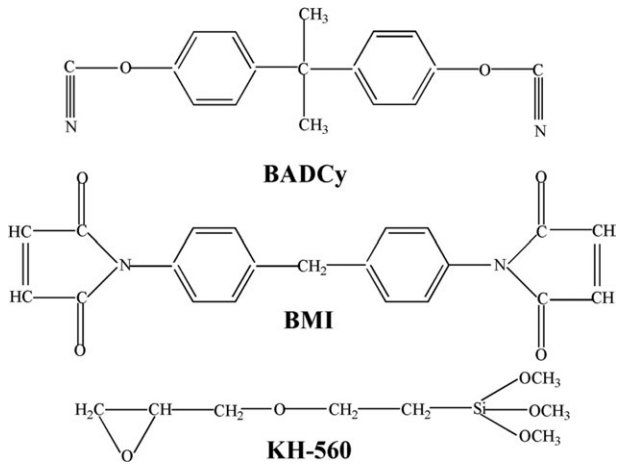

Figure 1. Chemical structures of BADCy, BMI, and KH-560.

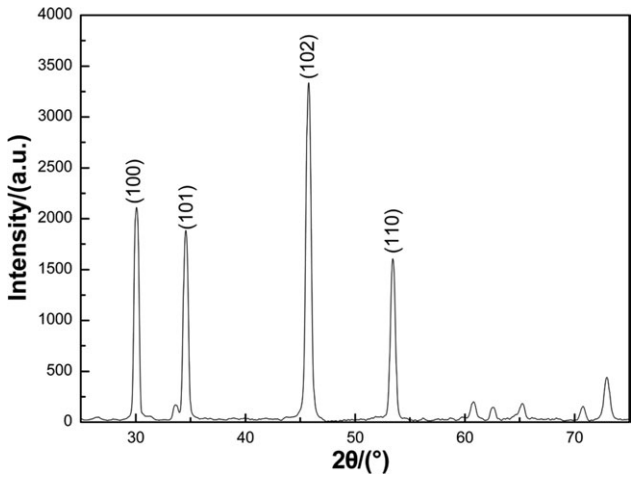

Figure 3. XRD pattern of NiS catalyst.

Preparation of CMCs. The surface of the graphite block covered NiS catalyst was put into silica tube. First, the silica tube could be filled with nitrogen gas to discharge the air of the furnace. The reaction furnace lining was heated to 700–800°C and kept under the same temperature for 0.5 h. Then, hydrogen was added into the silica tube, and the acetylene was dissolved in thiophene cylinders before it was added into the silica tube. The reaction time of the graphite block was 1.5 h. After cooling to room temperature, the CMCs were obtained.

Preparation of CMCs/BMI/BADCy ECA. The CMCs/BMI/BADCy ECA was prepared by the following steps: first, appropriate amounts of bisphenol A dicyanate (BADCy) and bismaleimide (BMI) prepolymer were thoroughly blended at 170°C for 1 h with vigorous stirring; second, after cooling the prepolymer to 110°C, the CMCs which treated with the small molecule coupling agent KH-560 were added, and then the ternary mixture was maintained with stirring until a homogeneous liquid was obtained. The ECA was cured via the following curing procedure: 150°C/3 h + 180°C/3 h and post cured at 200°C/2 h. In this work, keeping the mass ratio of BMI (Honghu bismaleimide resin company, Hubei, China) and BADCy (Shangyu Shengda Chemical Industry Limited company, Zhejiang, china) as a constant was 1 : 2.[17] The chemical structures of related materials were represented in Figure 1.

Characterization

Characterization of NiS, CMCs, and CMCs/BMI/BADCy-Based ECA. The surface morphology of NiS (Nonferrous metal material limited company, Baoji, China), CMCs, and CMCs/BMI/BADCy-based ECA was studied using a scanning electron microscope (SEM; Quanta-200, FEI) performed at an operating voltage of 20 kV. The phase structures of the NiS and CMCs were detected by X-ray powder diffraction (XRD; D/Max2000PC, Chongqing, China). WQF-31 FTIR spectrometer (Ruili, Kunming, China) was used to record Fourier transform infrared (FTIR) spectra of the CMCs, BT resin, and CMCs/BMI/BADCy-based ECA.

Measurement of Electrical Properties. Sz-82 digital four probes resistance tester (Suzhou Electronic Equipment Factory, China) was used to measure the conductivities of the BT resin and CMCs/BMI/BADCy-based ECA.

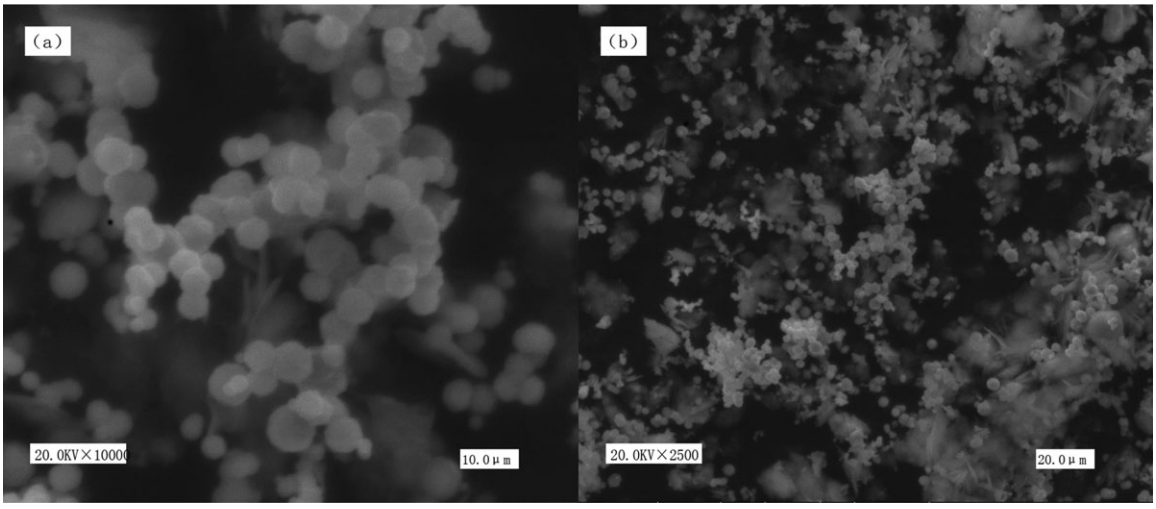

Figure 2. SEM images of NiS catalyst under varying magnifications.

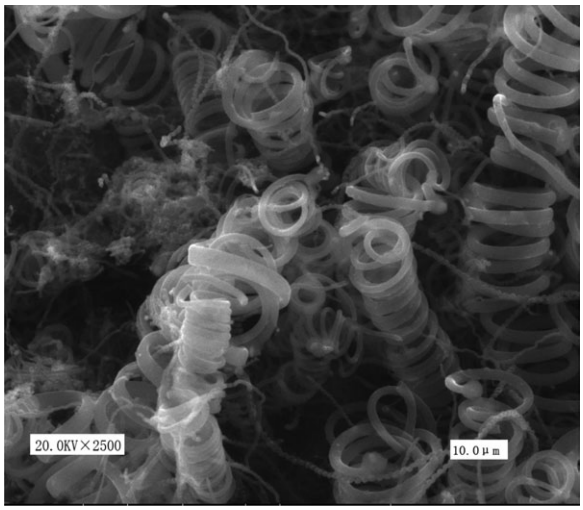

Figure 4. SEM images of the CMCs without thiophene.

Measurement of Mechanical Properties. The shear strength of the CMCs/BMI/BADCy-based ECA was measured with a Zwick universal material testing machine (Germany) at 25°C at a rate of 5 mm/min. For shear strength, a adhesive area of 25.0 × 12.0 mm^2 ECA was coated on the 45# silicon steel sheet. At least five specimens for each system were tested.

RESULTS AND DISCUSSION

Structures of NiS and CMCs

SEM image of NiS catalyst under varying magnifications was shown in Figure 2. We could find from this figure that the shape of the catalyst was sphere or spheroid. The catalyst surface was smooth and the diameter was 1–2 micrometers. Powder XRD analysis was used to indentify the phase structures. The XRD pattern of NiS catalyst particle was shown in Figure 3, which exhibited the standard NiS reflections. Nine diffraction peaks could be observed in Figure 3 and indexed to the (100), (101), (102), (110), (103), (200), (201), (004), and (202) planes of the hexagonal phase of NiS structure. The lattice constant of

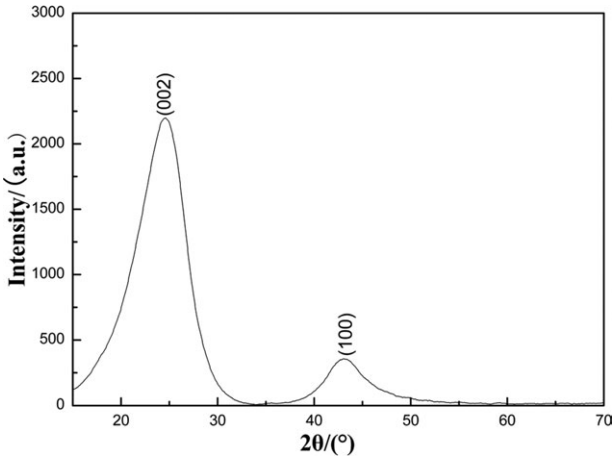

Figure 6. XRD pattern of CMCs.

NiS catalyst was $a = 3.426$ Å, $c = 5.321$ Å, which were similar to the reported the standard ($a = 3.425$ Å, $c = 5.340$ Å) (JCPDS, Card No.653419). Beyond that, it was observed that there was no impurities' peak. The results showed that the synthetic NiS catalyst had high purity and crystallization.

CMCs were prepared by the catalyst pyrolytic acetylene. SEM images of CMCs without thiophene were shown in Figure 4. From the Figure 4, it was observed that the morphology of CMCs was the double spiral structure. Sedimentation rates on the surface of the catalyst were different because of using sulfur as catalyst, which showed obvious anisotropy with the growth of the CMCs and low yield. To improve the quality and yield of CMCs, thiophene, a highly common substance, was added into the acetylene served as a cocatalyst to the flow duct facility.

The melting point of NiS was higher than the reaction temperature without insufflating thiophene. So the surface of graphite substrate did not form the layers of solid solutions. The pyrolysis of acetylene tocarbon atoms which did not well adsorb the surface of the catalyst resulted in preparing the irregular shaped. Insufflating thiophene, the surface on carbon atoms well formed

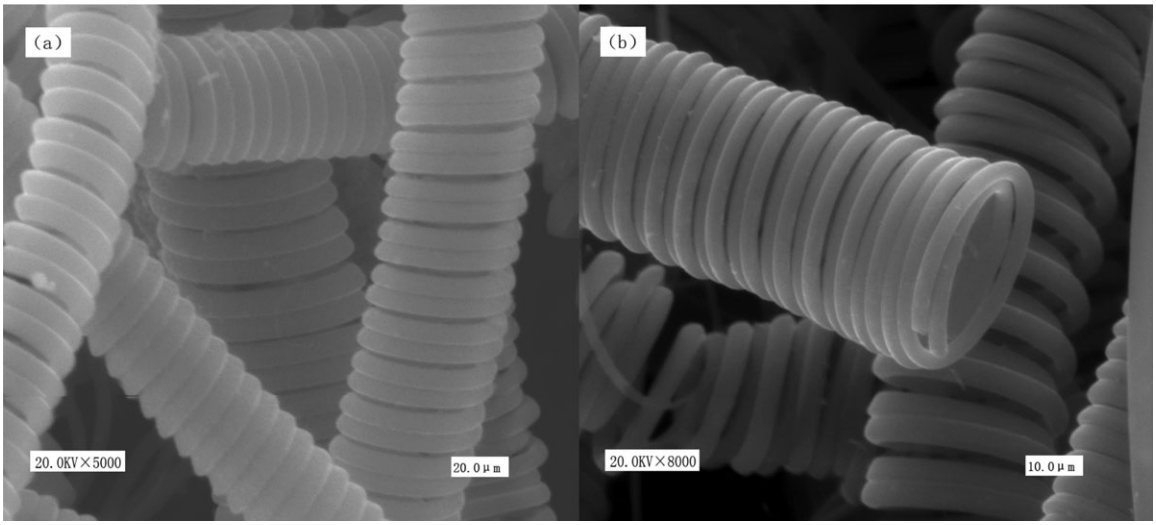

Figure 5. SEM images of the CMCs: (a) 5000 magnification (b) 8000 magnification.

Applied Polymer SCIENCE

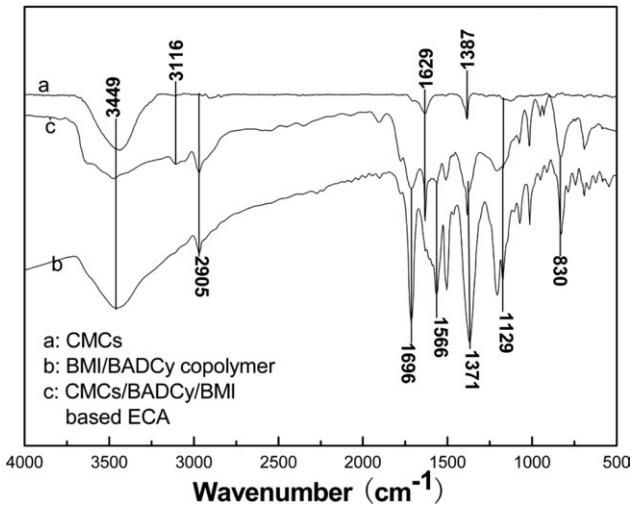

Figure 7. FTIR absorption spectra of CMCs, BT resin, and CMCs/BMI/BADCy-based ECA.

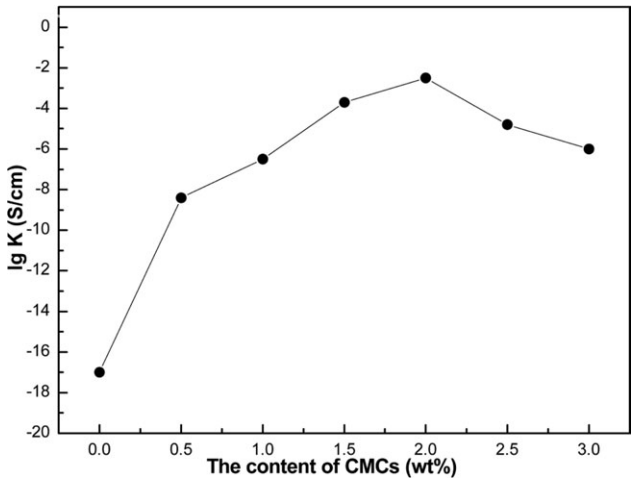

Figure 9. The electrical conductivity (K) of the CMCs/ BMI/BADCy-based ECA.

the layer of NI—S—C solid solutions as the CMCs growth point, so thiophene could improve considerably the quality and yield of CMCs. The rate of flow of acetylene was 10 sccm/min, which was lower than that of other domestic reportages.[18] So, the CMCs were prepared and the SEM images of the CMCs were shown in Figure 5. From the Figure 5, the helical microcarbon fibers were composed of two regular carbon fibers which showed the complicated twist structures. The spiral diameter and fiber diameter was 5–10 and 1 μm, respectively. The length of the spiral pipe reached millimeter level and the fiber showed the rectangular section. It had uniform screw diameter and screw pitch of the fiber. Simultaneity, more compact interfiber entanglement was almost the same as.

To further prove the structure of CMCs, the crystal structure of CMCs was analyzed by XRD shown in Figure 6. The reflections of XRD pattern could be indexed to the (002), (100), and (004). From the Figure 6, we could see two broad peaks at the 25.92° and 42.89° and hardly ever observed (004) diffraction peak around 54°. The interlayer spacing at 25.92° associated with (002) diffraction peak was 0.3988 nm, which was higher than the structure of graphite (0.3354 nm) and the disordered structure of graphite (0.3440 nm).[19] The result showed that the sample contained various microcrystals with different interlayer spacing. The sample contained a certain amount of amorphous carbon and lattice defects. From (002) diffraction peak, it indicated that the sample had high crystallinity and low degree of graphitization.

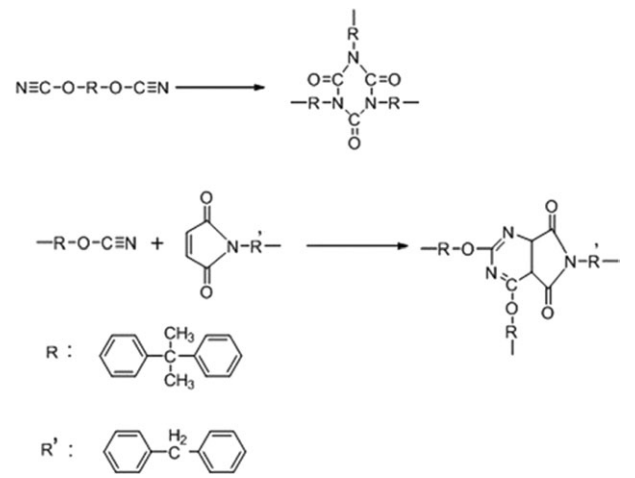

Figure 8. The polymerization mechanism of BMI/BADCy copolymer.

Structures of BT Resin and CMCs/BMI/BADCy-Based ECA

The FTIR spectra of CMCs/BMI/BADCy-based ECA were shown in Figure 7. For CMCs, the absorption peaks appeared at 3449, 1629, and 1706 cm^{-1} were ascribed to —O—H stretching vibration, —C=C— stretching vibration, and —C=O stretching vibration. The peak at 2905 and 1387 cm^{-1} could be attributed to —C—H stretching vibration which came from —CH_2— and —CH_3, respectively. For BT resin, the polymerization mechanism of BMI/BADCy was shown in Figure 8. According to the polymerization mechanism, absorption peaks appeared at 1566 and 1696 cm^{-1} in the polymer, which were ascribed to triazine stretching and isocyanate stretching, respectively. The peak at 1371 cm^{-1} could be attributed to pyrimidine stretching. The peak at 2238 and 1629 cm^{-1} disappeared which was —C≡N stretching vibration, and —C=C— stretching vibration, respectively. Compared to BT resin, the CMCs/BMI/BADCy-based ECA observed the —O—H stretching vibration, —C=C— stretching vibration, and —C=O stretching vibration. These evidences indicated that there was hydroxyl on the surface of CMCs and easy to form hydrogen bonding which form a strong interaction between CMCs and BT resin by KH-560. These peaks confirmed the synthesis of CMCs/BMI/BADCy-based ECA.

Conductivity Characteristics of CMCs/BMI/BADCy-Based ECA

The electrical conductivity (K) of the CMCs/BMI/BADCy-based ECA under various weight fractions of CMCs was observed in Figure 9. From the Figure 9, the electrical result was qualitative measurement that could show the relationship between electrical conductivity and the content of CMCs. It could be seen that the electrical conductivity of ECA increased gradually with the

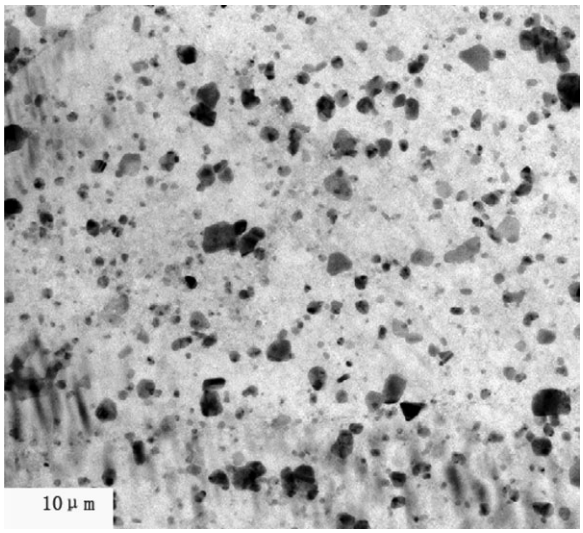

Figure 10. TEM micrograph of dispersion state CMCS in 2.0wt % CMCs/ BMI/BADCy-cured ECA.

conductive filler increasing. It indicated that the conductive adhesive had a good electrical conductivity when the CMCs were added into the modified system. The reason was that CMCs and BMI/BADCy copolymer were mutually isolated and they did not connect when the content of CMCs was low. Thus, the electrical conductivity of the CMCs/BMI/BADCy copolymer was mainly determined by BMI/BADCy copolymer. With increasing the content of CMCs, a local conductive network between CMCs and BMI/BADCy copolymer formed gradually, increasing the electrical conductivity. When the content of CMCs increased to 2.0 wt %, the electrical conductivity of the CMCs/BMI/BADCy copolymer increased significantly. The reason was that local conductive network between CMCs and BMI/BADCy copolymer had formed, which bring about dramatic increases in the conductivity channel. Figure 10 showed the distribution of CMCs in the 2.0 wt % CMCs/BMI/BADCy copolymer-cured ECA. From the Figure 10, it was observed that CMCs were homogeneous distribution into 2.0 wt % CMCs/BMI/BADCy copolymer. The black grain represented the CMCs, and the light coloring areas were BMI/BADCy copolymer. It could be seen that from the transmission electron microscope (TEM) image, on the one hand, many CMCs existed throughout the polymer matrix and the compatibility between CMCs and BMI/BADCy copolymer was good enough to obtain homogeneously dispersion. Thus, the electrical conductivity increased to 3.16×10^{-2} S/cm which was 15 orders of magnitude higher than that of the BT rein (about 10^{-17} S/cm). However, when the filler content was 2.5 and 3 wt %, the electrical conductivity of the ECA was 1.78×10^{-5} S/cm and 1.32×10^{-6} S/cm, respectively. The reason was that the ECA possessed nonhomogeneous particle distribution and CMCs agglomeration, reducing its electrical conductivity.

Mechanical Properties of CMCs/ BMI/BADCy-Based ECA

The mechanical properties were a crucial factor that dictated the suitability of the composite to be applied in electronic packaging. Figure 11 showed that shear strength of ECA between 25 and 200°C increased when the content of the filler increased from 0 to 1.5 wt %, and then gradually decreased with the increase of the filler content when it was more than 1.5 wt %. When the CMCs content in CMCs/ BMI/BADCy-based ECA was 1.5 wt %, the shear strength between 25 and 200°C reached maximum value of 22.8 and 21.4 MPa, respectively. The maximum shear strength between 25 and 200°C was 1.12 and 1.18 times of the value for modified BMI/BADCy resins, respectively. The change could be explained as follows. Traditionally, the dispersion of particles in polymeric materials had proven difficult and frequently led to phase separation and agglomeration. The deterioration of the shear strength of composites was believed to be related mainly to the poor interfacial adhesion between filler and BT resin, which results in many defects and flaws in the composites.

As for shear strength, it is known that the shear strength involves cohesive strength of the ECA. For high temperature resistant adhesive, with the increases of the filler, the cohesive strength would increase due to filler improved rigidity of the polymer chains. However, when the content of CMCs was more than 1.5 wt %, the filler could not disperse well in the conductive adhesive, reducing its shear strength. It is noteworthy that the introduction of CMCs particle into the BT resin largely increases the shear strength properties, as compared with that of BT resin. Consequently, for the shear strength of CMCs/ BMI/BADCy, the optimum content of CMCs was 1.5 wt %.

CONCLUSIONS

A new class of ECA filled with CMCs as conductive filler, which was synthesized by the catalytic decomposition of acetylene using nickel sulfide particles as the catalyst which prepared by solvothermal method. By mixing the coupling agent (KH-560)-treated CMCs, bismaleimide resin, cyanate ester resin, and other additives in proportion, the CMCs/BMI/BADCy-based ECA was obtained successfully, which could be cured by the following curing schedule: 150°C/3 h + 180°C/3 h, and then post cured at 200°C/2 h. The electrical conductivity of the CMCs/BMI/BADCy-based ECA increased first as the conductive filler

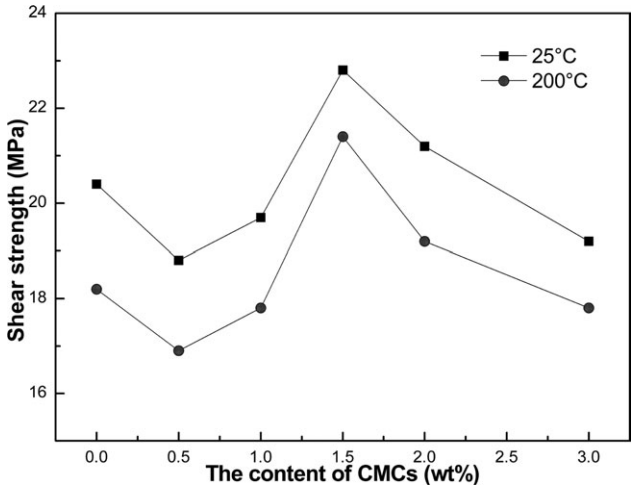

Figure 11. Mechanical properties of CMCs/ BMI/BADCy-based ECA.

increased. It reached the highest value at 3.16×10^{-2} S/cm when the content of CMCs was 2 wt % and then decreased. The increase of the shear strength of ECA joint to 45# silicon steel sheet with an increase in filler content was observed. The shear strength of the CMCs/BMI/BADCy-based ECA remained at a high value when the content of the CMCs was 1.5 wt %.

ACKNOWLEDGMENTS

This work was supported by a grant from the Graduate Starting Seed of Northwestern Polytechnical University (grant numbers: Z2011010, Z2012153).

REFERENCES

1. Kim, J. M.; Yasuda, K.; Fujimoto, K. *J. Electron. Mater.* **2005,** *34*, 600.
2. Mir, I.; Kumar, D. *Int. J. Adhes. Adhes.* **2008,** *28*, 362.
3. Yacobi, B. G.; Martin, S.; Davis, K.; Hudson, A.; Hubert, M. Adhesive bonding in microelectronics and photonics. *J. Appl. Phys.* **2002,** *91*, 6227.
4. Xiao, J.; Chung, D. D. L. *J. Electron. Mater.* **2005,** *34*, 625.
5. Zhao, H. S.; Liang, T. X.; Liu, B. *Int. J. Adhes. Adhes.* **2007,** *27*. 429.
6. Chen, D. P.; Qiao, X. L.; Qiu, X. L.; Tan, F. T.; Chen, J. G.; Jiang, R. Z. *J. Mater. Sci. Mater. Electron.* **2010,** *21*, 486.
7. Novak, I., Krupa, I. *Eur. Polym. J.* **2004,** *40*, 1417.
8. Yang, S. M.; Chen, X. Q.; Motojima, S. J.; Ichihara M. *Carbon* **2005,** *43*, 827.
9. Motojima, S.; Itoh, Y.; Asakura, S.; Iwanaga, H. *J. Mater. Sci.* **1995,** *30*, 5049.
10. Chen, X.Q.; Motojima, S. *Carbon* **1999,** *37*, 1817.
11. Kuzuya, C.; Hwang, W. I.; Hirako, S.; Hishikawa, Y.; Motojima, S. *Chem. Vapor. Depos.* **2002,** *8*, 57.
12. Chen, X. Q.; Yang, S. M.; Motojima, S. *Mater. Lett.* **2002,** *57*, 48.
13. Zhang, M.; Nakayama, Y.; Pan, L. *Jpn. J. Appl. Phys.* **2000,** *39*, 1242.
14. Takikawa, H.; Miyano, R.; Yatsuki, M.; Sakakibara T. *Jpn. J. Appl. Phys.* **1998,** *37*, 187.
15. Tan, F. T.; Qiao, X. L.; Chen, J. G.; Wang, H. S. *Int. J. Adhes. Adhes.* **2006,** *26*, 406.
16. Inoue, M.; Muta, H.; Maekawa, T.; Yamanaka, S.; Suganuma, K. *J. Electron. Mater.* **2009,** *38*, 2013.
17. Fang, F.; Yan, H. X.; Zhang, J. P. *Polym. Mater. Sci. Eng.* **2007,** *23*, 222.
18. Bi, H.; Kou, K. C.; Zhang, J. Q. *J. Synth. Cryst.* **2007,** *36*, 559.
19. Li, C. J.; Ma, B. X.; Huo, X. X. *Adv. Carbons* **1999,** *14*, 19.